Cell Reports

Article

TRIP13 Functions in the Establishment of the Spindle Assembly Checkpoint by Replenishing O-MAD2

Graphical Abstract

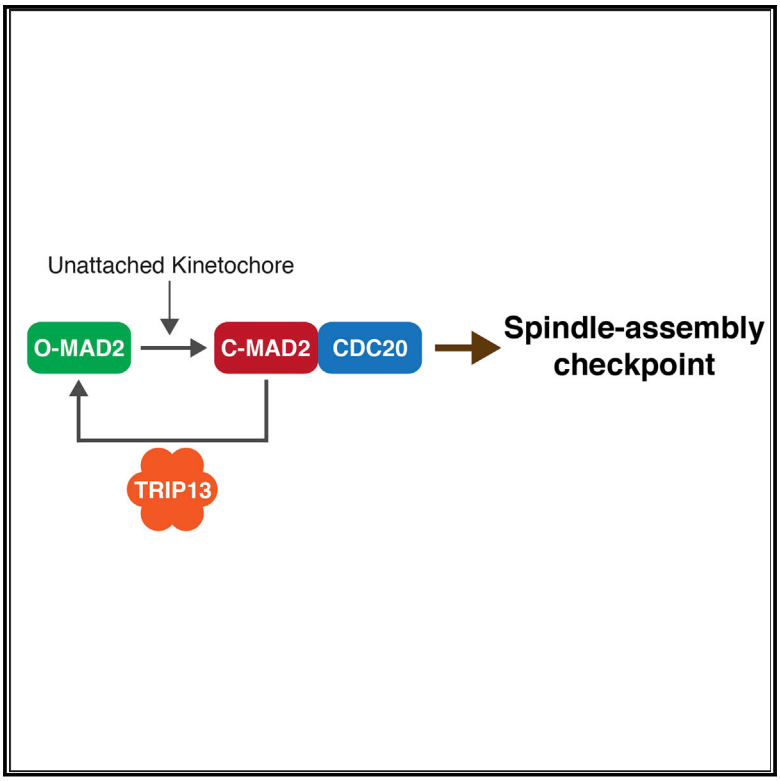

Authors

Hoi Tang Ma, Randy Y.C. Poon

Correspondence

rycpoon@ust.hk

In Brief

C-MAD2 is required for the activation of the spindle assembly checkpoint. Ma and Poon show that C-MAD2 alone is insufficient to support the spindle assembly checkpoint. TRIP13 is involved in replenishing the O-MAD2 pool for conversion into C-MAD2 and the activation of the spindle assembly checkpoint.

Highlights

- TRIP13-deficient cells are unable to activate the spindle assembly checkpoint
- TRIP13-deficient cells contain only C-MAD2
- C-MAD2 alone is insufficient to enable the spindle assembly checkpoint
- TRIP13 replenishes the O-MAD2 pool for activation of the SAC

Ma & Poon, 2018, Cell Reports *22*, 1439–1450
February 6, 2018
https://doi.org/10.1016/j.celrep.2018.01.027

CellPress

Cell Reports
Article

TRIP13 Functions in the Establishment of the Spindle Assembly Checkpoint by Replenishing O-MAD2

Hoi Tang Ma[1] and Randy Y.C. Poon[1,2,*]
[1]Division of Life Science, Center for Cancer Research, and State Key Laboratory of Molecular Neuroscience, Hong Kong University of Science and Technology, Clear Water Bay, Hong Kong
[2]Lead Contact
*Correspondence: rycpoon@ust.hk
https://doi.org/10.1016/j.celrep.2018.01.027

SUMMARY

The spindle assembly checkpoint (SAC) prevents premature segregation of chromosomes during mitosis. This process requires structural remodeling of MAD2 from O-MAD2 to C-MAD2 conformation. After the checkpoint is satisfied, C-MAD2 is reverted to O-MAD2 to allow anaphase-promoting complex/cyclosome (APC/C) to trigger anaphase. Recently, the AAA$^+$-ATPase TRIP13 was shown to act in concert with p31^{comet} to catalyze C- to O-MAD2. Paradoxically, although C-MAD2 is present in TRIP13-deficient cells, the SAC cannot be activated. Using a degron-mediated system to uncouple TRIP13 from O- and C-MAD2 equilibrium, we demonstrated that the loss of TRIP13 did not immediately abolish the SAC, but the resulting C-MAD2-only environment was insufficient to enable the SAC. These results favor a model in which MAD2-CDC20 interaction is coupled directly to the conversion of O- to C-MAD2 instead of one that involves unliganded C-MAD2. TRIP13 replenishes the O-MAD2 pool for activation by unattached kinetochores.

INTRODUCTION

Sister chromatid segregation and mitotic exit are driven by a ubiquitin ligase called anaphase-promoting complex/cyclosome (APC/C) with its targeting subunit CDC20 (Primorac and Musacchio, 2013). Activation of APC/C^{CDC20} is initiated only when all the chromosomes have attached properly to the bipolar spindle. Unattached kinetochores or the lack of tension between the paired kinetochores activates a surveillance mechanism, termed the spindle assembly checkpoint (SAC), which inhibits the APC/C^{CDC20} (Musacchio, 2015). The SAC ensures that mitotic exit only occurs after all the chromosomes have achieved proper bipolar spindle attachment.

Activation of the SAC involves the assembly of a Mitotic Checkpoint Complex (MCC) containing MAD2, BUBR1, BUB3, and CDC20, which binds APC/C^{CDC20} (containing a second CDC20) and suppresses its activity (Izawa and Pines, 2015; Alfieri et al., 2016; Yamaguchi et al., 2016; Primorac and Musacchio, 2013). Binding to APC/C^{CDC20} requires a structural change in MAD2 from an open conformation (known as O-MAD2) to a more stable closed conformation (C-MAD2) (Luo et al., 2002). Upon this structural remodeling, the C-terminal CDC20-binding site is exposed, allowing C-MAD2 to interact with CDC20 (Mapelli et al., 2007). According to a MAD2 template model, the C-MAD2 binding to MAD1 at kinetochores serves as a template for converting O-MAD2 into C-MAD2 (De Antoni et al., 2005). The new C-MAD2 then dissociates from the kinetochores and forms MCC, which in turn serves as a template for converting more O-MAD2 to C-MAD2 in the cytosol. MPS1-catalyzed phosphorylation of KNL1, BUB1, and MAD1 is critical for O- to C-MAD2 conversion (Ji et al., 2017; Faesen et al., 2017).

After the SAC is satisfied, C-MAD2 is reverted to O-MAD2 to allow APC/C^{CDC20} to drive anaphase. One mechanism involves the binding of C-MAD2 to p31^{comet} (also called MAD2L1BP) (Habu et al., 2002), a protein with a similar structure as C-MAD2 (Yang et al., 2007). On the one hand, binding of p31^{comet} to C-MAD2 blocks O-MAD2–C-MAD2 dimerization, thereby preventing MAD2 activation (Mapelli et al., 2006; Yang et al., 2007). On the other hand, p31^{comet} assists in converting the preexisting C-MAD2 back to O-MAD2 by a p31^{comet}-interacting protein called TRIP13 (Eytan et al., 2014; Wang et al., 2014). TRIP13 is an AAA$^+$-ATPase that also functions in various processes including meiotic DNA break formation and recombination, checkpoint signaling, and chromosome synapsis (Vader, 2015). Binding of p31^{comet} to the N-terminal domain of TRIP13 positions the disordered MAD2 N terminus to interact with TRIP13, allowing TRIP13 to promote structural changes in MAD2 (Ye et al., 2017). In agreement with the importance of TRIP13 in regulating chromosomal stability, individuals with loss-of-function mutations in TRIP13 show dysregulated SAC and are predisposed to Wilms tumor (Yost et al., 2017).

Surprisingly, our recent study using TRIP13- and/or p31^{comet}-deficient cell lines indicated that neither TRIP13 nor p31^{comet} is essential for mitotic exit (Ma and Poon, 2016). Recent reports of p31^{comet}-knockout mice and *C. elegans* TRIP13 mutants also agreed with this observation (Choi et al., 2016; Nelson et al., 2015). We found that TRIP13 (but not p31^{comet}) is essential for converting C-MAD2 to O-MAD2 in the cell, as the conformation of MAD2 switched from predominantly O-MAD2 in wild-type cells to exclusively C-MAD2 in TRIP13-deficient cells.

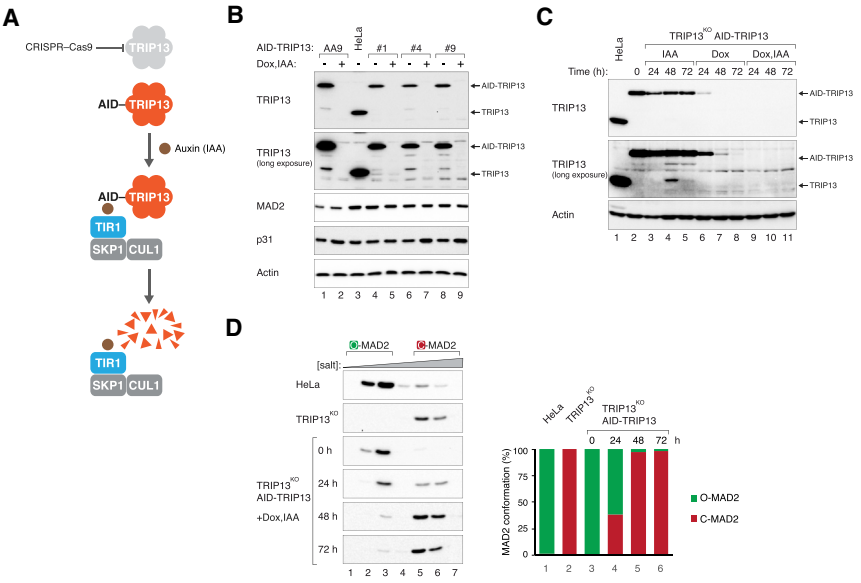

Figure 1. Degron-Mediated Depletion of TRIP13 Leads to C-MAD2 Accumulation

(A) Auxin-inducible degron (AID)-TRIP13 system. In response to IAA, AID-TRIP13 is rapidly targeted to degradation in cells expressing the ubiquitin ligase SCF^{TIR1}. HeLa cells were infected with retroviruses expressing AID-TRIP13 before being transfected with a CRISPR-Cas9 construct targeting endogenous TRIP13 (at the UTR-open reading frame [ORF] boundary; hence, AID-TRIP13 was not targeted). The cells were then infected with retroviruses expressing TIR1. Individual clones lacking endogenous TRIP13 and expressing AID-TRIP13 were then isolated.

(B) Inducible deficiency of TRIP13. Control HeLa and individual clones of $TRIP13^{KO}$ cells expressing AID-TRIP13 were grown in the presence or absence of IAA and Dox for 24 hr before being harvested. Lysates were prepared and the indicated proteins were detected with immunoblotting. Equal loading of lysates was confirmed by immunoblotting for actin. Clone AA9 was generated by first transfecting CRISPR-Cas9 before infecting with the AID-TRIP13 and TIR1-myc constructs. Clones 1, 4, and 9 were generated by the opposite order. Unless stated otherwise, data from clone 9 are shown in this study.

(C) TRIP13 is effectively depleted using IAA and Dox. $TRIP13^{KO}$ expressing AID-TRIP13 were grown in the presence of IAA and/or Dox and harvested at the indicated time. Lysates were prepared and the expression of TRIP13 was detected using immunoblotting. Lysates from control HeLa cells were loaded in lane 1 to indicate the position of endogenous TRIP13. Equal loading of lysates was confirmed by actin analysis.

(D) Progressive accumulation of C-MAD2 after TRIP13 depletion. $TRIP13^{KO}$ expressing AID-TRIP13 was treated with IAA and Dox and harvested at the indicated time points. Lysates were prepared and MAD2 conformation was analyzed using ion exchange chromatography. Fractions were eluted with buffer containing different concentrations of salt and analyzed with immunoblotting for MAD2. The fractions corresponding to O-MAD2 and C-MAD2 are indicated at the top. Lysates from HeLa and $TRIP13^{KO}$ were included as controls. The relative abundance of O-MAD2 and C-MAD2 was quantified and plotted (right-hand panel).

Paradoxically, these TRIP13-deficient cells cannot be arrested in mitosis with spindle-disrupting agents (Ma and Poon, 2016). This surprising result was further corroborated by studies using other TRIP13-deficient cells (Marks et al., 2017; Yost et al., 2017). One possibility is that TRIP13 itself is actually an integral part of the SAC machinery. Another possibility is that TRIP13 plays a more indirect role in SAC activation: as TRIP13-deficient cells contain exclusively C-MAD2, it is possible that C-MAD2 alone is insufficient to enable the SAC. As ablating TRIP13 inevitably results in the accumulation of C-MAD2, it is not possible to simply use TRIP13-deficient cells to distinguish these possibilities. In this study, we addressed this problem by using a degron-mediated system to induce TRIP13 deficiency, thereby allowing us to temporally uncouple TRIP13 from O- and C-MAD2 equilibrium.

RESULTS

TRIP13 Is Not Directly Involved in SAC Activation

To generate an inducible TRIP13 deficiency system, we used CRISPR-Cas9 to knock out TRIP13 while rescuing the cells with an auxin-inducible degron (AID)-tagged TRIP13 (Figure 1A). This allowed robust and near-complete removal of TRIP13 in response to plant auxin (or indole-3-acetic acid [IAA]) in cells expressing the ubiquitin ligase SCF^{TIR1} at defined windows during the cell cycle (Nishimura et al., 2009).

Individual clones lacking endogenous TRIP13 ($TRIP13^{KO}$) and expressing AID-TRIP13 were then isolated (Figure 1B). The AID-TRIP13 was expressed at a similar concentration as the endogenous TRIP13 in parental cells. We found that the order of knocking out TRIP13 and expressing AID-TRIP13 did not affect the generation of the cell lines. However, the addition of IAA alone was unable to completely remove AID-TRIP13 (Figure S1A) and did not significantly affect MAD2 conformation equilibrium in the cell (Figure S1B). As the AID-TRIP13 was under the control of a Tet-Off promoter, the expression of AID-TRIP13 could be further suppressed with doxycycline hydrochloride (Dox). Figure 1C shows that AID-TRIP13 was efficiently removed after incubating the cells with IAA and Dox together.

A spin column-based ion exchange chromatography was adopted to analyze the conformation of MAD2 in the presence or absence of TRIP13 (Ma and Poon, 2016). O- and C-MAD2 were eluted with relatively low and high salt concentrations, respectively. In accordance with previous studies (Luo et al., 2004), endogenous MAD2 was present predominantly as O-MAD2 in control cells. Because TRIP13 is involved in C- to O-MAD2 conversion, $TRIP13^{KO}$ cells contained exclusively C-MAD2 (Figure 1D). Similar to control HeLa cells, $TRIP13^{KO}$ expressing AID-TRIP13 contained mainly O-MAD2. The O-MAD2 only progressively shifted to C-MAD2 after AID-TRIP13 was degraded (Figure 1D). Hence, this system was able to provide a window of time (between 24 and 48 hr) when TRIP13 was absent while O-MAD2 was still present.

To see if TRIP13 is required for activating the SAC, AID-TRIP13 was targeted to degradation before the cells were incubated with the spindle-disrupting agent nocodazole (NOC). As expected, NOC induced a mitotic arrest in cells containing either endogenous TRIP13 or AID-TRIP13 (as indicated by the phosphorylation

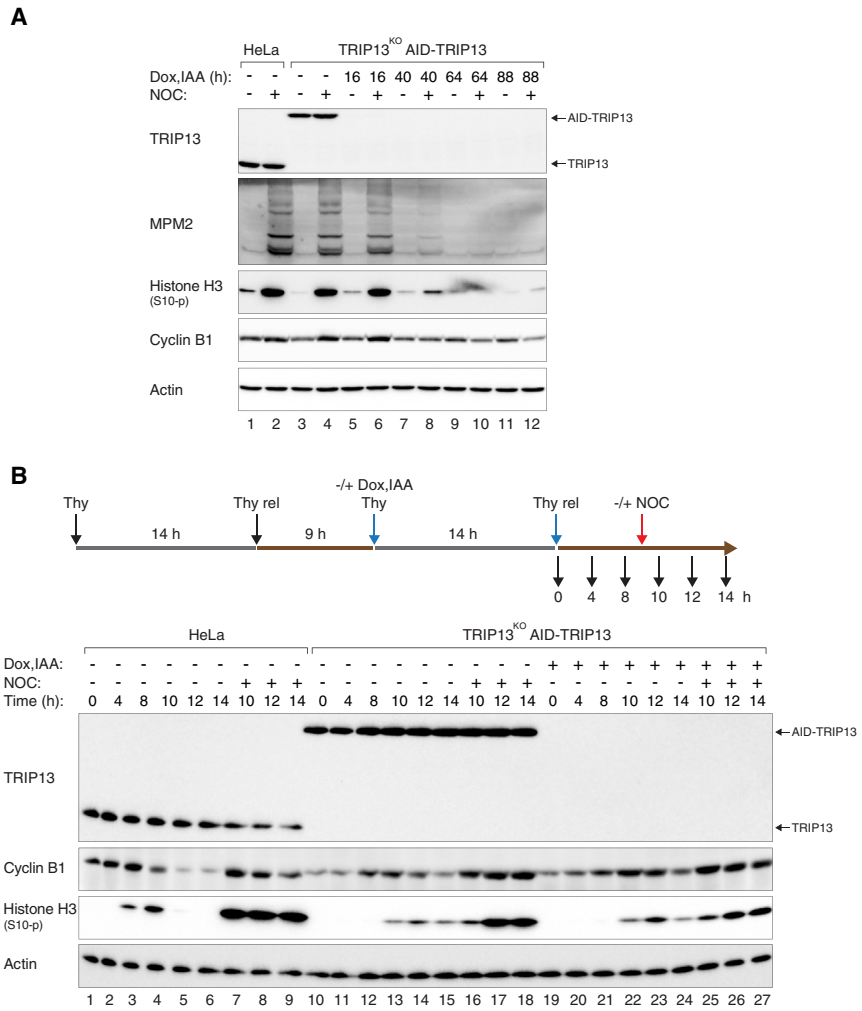

Figure 2. TRIP13 Is Not Required for Activating the SAC

(A) Cells can be arrested in mitosis immediately after the degradation of TRIP13. HeLa or AID-TRIP13-expressing TRIP13^{KO} cells were treated with buffer or IAA and Dox for the indicated time. Buffer or NOC was then added for 16 hr before the cells were harvested. TRIP13 and mitotic markers (MPM2, histone H3^{Ser10} phosphorylation, and cyclin B1) were then detected with immunoblotting. Equal loading of lysates was confirmed by immunoblotting for actin.

(B) Synchronized TRIP13-deficient cells can be blocked in mitosis with NOC. A schematic diagram of the double-thymidine synchronization procedure is shown at the top. IAA and Dox were added when the second thymidine block was applied to turn off the expression of AID-TRIP13 (and remained for the rest of the experiment). The cells were harvested at the indicated time points. Lysates were prepared and analyzed with immunoblotting.

of mitotic epitopes MPM2 and histone H3^{Ser10}) (Figure 2A). Cells were also able to be trapped in mitosis shortly after AID-TRIP13 was targeted to degradation, but not after prolonged removal of TRIP13. The delayed loss of the SAC after AID-TRIP13 was degraded suggested that TRIP13 itself is not directly involved in the activation of the SAC.

To examine the relationship between TRIP13 and the SAC more stringently, cells were synchronized with a double-thymidine procedure before being exposed to IAA and Dox during the second thymidine block (Figure 2B). Although the cells contained no detectable TRIP13 before entering mitosis, they were able to be enriched in mitosis with NOC. Analysis with ion exchange chromatography indicated that the synchronized TRIP13-deficient cells still contained a substantial fraction of O-MAD2 during G_2 phase (Figure 3A). Although a portion of O-MAD2 was subsequently converted into C-MAD2 after the cells passed through mitosis, O-MAD2 was still present during the next G_1 phase.

We next analyzed the level of MCC by immunoprecipitating MAD2 (Figure 3B). As expected, MAD2-CDC20 complexes were absent during G_2 phase but accumulated in mitosis. Importantly, MAD2-CDC20 complexes accumulated in mitosis even after TRIP13 was degraded. Similarly, binding of MAD2 and CDC20 to BUBR1 or APC/C was unaffected after AID-TRIP13 was degraded (Figure S2).

As others and our group have observed previously (Ma and Poon, 2016; Yost et al., 2017), depletion of TRIP13 resulted in an accumulation of p31^{comet} (Figure 3B). In the absence of TRIP13, the interaction between MAD2 and p31^{comet} could readily be detected during both G_2 and mitosis. By contrast, the interaction between MAD2 and MAD1 was similar in the presence or absence of TRIP13, indicating that the C-MAD2 in TRIP13^{KO} cells was able to bind MAD1. Interesting, more MAD1 was found in the p31^{comet} immunoprecipitates from TRIP13^{KO} cells than from TRIP13-expressing cells (Figure 3B, lanes 11 and 12). Converse immunoprecipitation of MAD1 confirmed the increase in p31^{comet}-MAD1 complexes in TRIP13^{KO} cells (Figure 3C). These results indicated that MAD1-MAD2-p31^{comet} complexes were enriched in the absence of TRIP13.

To ensure that the potential functions of TRIP13 on the SAC were not compensated by the accumulated p31^{comet}, we next generated AID-TRIP13-expressing cells in a background lacking both TRIP13 and p31^{comet} (TRIP13^{KO} p31^{KO}). As before, degradation of AID-TRIP13 (Figure S3A) resulted in the conversion of O-MAD2 to C-MAD2 (Figure S3B). However, as we have previously discovered in p31^{KO} cells (Ma and Poon, 2016), p31^{comet} deficiency already induced a partial increase in C-MAD2. Hence the window of time of which the cells contained no AID-TRIP13 but still contained O-MAD2 was smaller than in TRIP13^{KO} cells. Nevertheless, the cells were able to be blocked in mitosis with NOC (Figure S3C), indicating that p31^{comet} did not play an essential role in SAC activation in the absence of TRIP13.

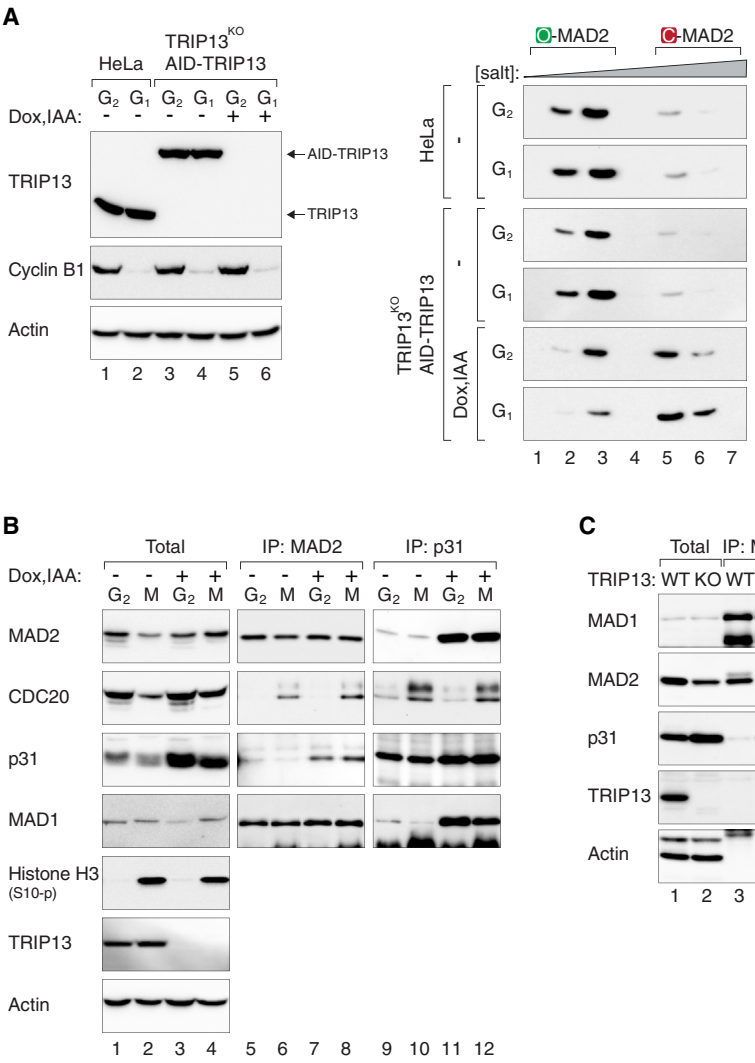

Figure 3. Formation of the MCC Does Not Require TRIP13

(A) O-MAD2 is present during G_2 in synchronized TRIP13^{KO} cells. TRIP13^{KO} expressing AID-TRIP13 was synchronized with a double-thymidine procedure. AID-TRIP13 was degraded by the addition of IAA and Dox at the second thymidine block. Cells at G_2 and G_1 were collected at t = 8 hr and t = 15 hr, respectively, after releasing from the second thymidine block. Lysates were prepared and analyzed with immunoblotting (left-hand panel). The expression of cyclin B1 indicated the effectiveness of the synchronization. The conformation of MAD2 in the lysates was also analyzed using ion exchange chromatography as in Figure 1D (right-hand panel).

(B) MCC can be formed in both the presence and absence of TRIP13. TRIP13^{KO} expressing AID-TRIP13 was synchronized as described in (A). The G_2 cells were further incubated with NOC for 4 hr to obtain mitotic cells (M). The level of MCC in G_2 and mitotic cells was analyzed by MAD2 immunoprecipitation. Lysates were also immunoprecipitated using antibodies against p31^{comet}. Both the total lysates and immunoprecipitates were analyzed with immunoblotting. Histone H3^{Ser10} phosphorylation confirmed that the cells were blocked in mitosis with or without TRIP13.

(C) Ablation of TRIP13 increases the binding of p31^{comet} to MAD1-MAD2. Lysates from HeLa (wild-type [WT]) and TRIP13^{KO} (knockout [KO]) were prepared and subjected to immunoprecipitation with antibodies against MAD1. Both the total lysates and the immunoprecipitates were then analyzed with immunoblotting.

Collectively, the delayed loss of the SAC after TRIP13 is eliminated indicates that the role of TRIP13 itself on the SAC may be an indirect one.

The Loss of the SAC in the Absence of TRIP13 Is Inextricably Linked to the Depletion of O-MAD2

To examine the relationship between the ratio of O-MAD2:C-MAD2 and the ability to activate the SAC, TRIP13^{KO} cells expressing AID-TRIP13 were synchronized with a double-thymidine procedure and treated with IAA and Dox at various time points before G_2 (Figure 4A). A CDK1 inhibitor was used to trap the cells in G_2 before the MAD2 conformation was analyzed. Figure 4B shows that, when the cells reached G_2, AID-TRIP13 was effectively eliminated by the IAA and Dox added at various time points between 12 and 49 hr earlier. Analysis of MAD2 conformation revealed that O-MAD2 was present when AID-TRIP13 was degraded at relatively late time points (at or after the second thymidine block was applied), but not following more prolonged degradation of AID-TRIP13 (Figure 4B). Importantly, when the cells were released from G_2 into a mitosis (NOC and the proteasome inhibitor MG132 were added to prevent cells from exiting mitosis immediately), the ability of MAD2 to interact with CDC20 progressively decreased, correlating with the time after AID-TRIP13 was degraded (Figure 4C). These results indicated that the formation of MAD2-CDC20 complexes correlated with the level of O-MAD2.

O-MAD2 Is Essential for SAC Activation

To test the hypothesis that the presence of O-MAD2 is required for activating the SAC, we next performed experiments that introduced O-MAD2 into TRIP13-deficient cells. HA-MAD2 (which could be distinguished from endogenous MAD2 by gel mobility) was transiently transfected into HeLa and TRIP13^{KO} cells (Figure 5A). While the endogenous MAD2 in TRIP13^{KO} cells was present exclusively as C-MAD2, the ectopically expressed HA-MAD2 was present as both O-MAD2 and C-MAD2 (Figure 5B). This is consistent with the idea that MAD2 is first folded into O-MAD2 following synthesis (Skinner et al., 2008), and that overexpressed MAD2 can increase the O-MAD2 population (Marks et al., 2017). By contrast, both endogenous MAD2 and HA-MAD2 contained the O-MAD2 form in control HeLa cells. In the control cells, both MAD2

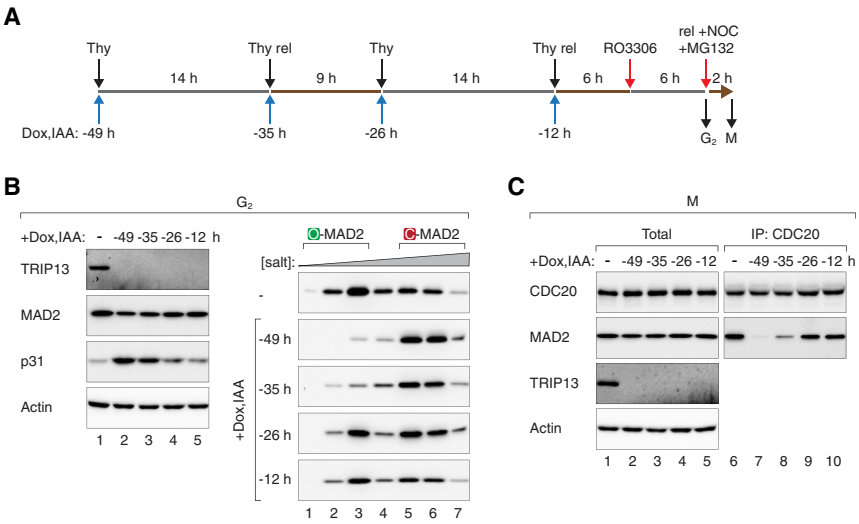

Figure 4. The Level of MAD2-CDC20 Complexes during Mitosis Correlates with the Presence of O-MAD2

(A) Initiating AID-TRIP13 destruction at different time before mitosis. TRIP13^{KO} expressing AID-TRIP13 was synchronized with a double-thymidine procedure. At different time points, IAA and Dox were added to degrade AID-TRIP13. The cells were incubated with a CDK1 inhibitor (RO3306) at 6 hr after the second thymidine release to trap the cells at G_2 (harvested 6 hr later). Flow cytometry analysis of cells treated with IAA and Dox at different time points are shown in Figure S4. A portion of cells was released from the RO3306 block and incubated with NOC and MG132 to arrest them in mitosis (harvested by mechanical shakeoff 2 hr later).

(B) C-MAD2 increased progressively after AID-TRIP13 was destroyed. AID-TRIP13 was destroyed at different time points and harvested at G_2 as described in (A). Lysates were prepared and the indicated proteins were detected with immunoblotting (left-hand panel). MAD2 conformation was analyzed using ion exchange chromatography as in Figure 1D (right-hand panel).

(C) The level of MAD2-CDC20 complexes during mitosis correlates with the abundance of O-MAD2. AID-TRIP13 was destroyed at different time points and harvested at mitosis as described in (A). Lysates were prepared and subjected to immunoprecipitation with antibodies against CDC20. Both the total lysates and the immunoprecipitates were then analyzed with immunoblotting.

and HA-MAD2 could bind CDC20 during mitosis (Figure 5A; more MAD2 than HA-MAD2 was co-immunoprecipitated because HA-MAD2 was expressed only in a fraction of the cells by transient transfection). HA-MAD2 was also enriched in CDC20 immunoprecipitates from TRIP13^{KO} cells (while endogenous MAD2 could only bind weakly), suggesting that the newly synthesized O-MAD2 could form MCC.

To examine if the ectopically expressed HA-MAD2 could restore the SAC in TRIP13^{KO} cells, the transfected cells were treated with NOC and tracked using live-cell imaging (Figure 5C). While control HeLa cells could be enriched in mitosis with NOC for about 10 hr, TRIP13^{KO} cells exited mitosis rapidly. The defective SAC in the TRIP13^{KO} cells was at least partially re-established by expressing HA-MAD2. As shown previously (Ma and Poon, 2016), the duration of unperturbed mitosis also decreased after TRIP13 was ablated (Figure 5C, lower panel). Introduction of HA-MAD2 into TRIP13^{KO} cells also increased the unperturbed mitotic duration similar to that in control cells. We further verified that O-MAD2 could restore the SAC in TRIP13^{KO} cells by measuring the histone H3^{Ser10} phosphorylation in individual cells (Figure 5D). In agreement with the SAC loss in TRIP13^{KO} cells, histone H3^{Ser10} phosphorylation accumulated in control, but not TRIP13^{KO}, cells after NOC treatment. The increase in histone H3^{Ser10} phosphorylation was at least partially restored by the ectopically expressed HA-MAD2. By contrast, HA-MAD2 could not restore the SAC that was disrupted with an MPS1 inhibitor, indicating the effect was specific for TRIP13 deficiency (Figure S5).

We next examined if the MAD2^{V193N} mutant, which adopts only the O-MAD2 conformation (Mapelli et al., 2007), could restore the SAC in TRIP13^{KO} cells. Expression of wild-type HA-MAD2, but not MAD2^{V193N}, was able to increase histone H3^{Ser10} phosphorylation in NOC-treated TRIP13^{KO} cells (Figure S6). These data suggested that the ability to convert from O- to C-MAD2, rather than the presence of O-MAD2 alone, is important for establishing the SAC.

Our results are consistent with the hypothesis that the presence of C-MAD2 alone is insufficient to support the SAC. To test this hypothesis directly, we uncoupled MAD2 remodeling from TRIP13 by using a C-MAD2-specific mutant. The endogenous MAD2 was first disrupted with CRISPR-Cas9. Given that MAD2 is essential for cell survival, the MAD2^{KO} cells were supplemented with recombinant HA-MAD2. As the HA-MAD2 was under the control of a Tet-Off promoter, its expression could be turned off using Dox. Figure 6A shows that HA-MAD2 was expressed at a concentration similar to the endogenous MAD2 in HeLa cells. While the SAC could be activated with NOC in HA-MAD2-expressing MAD2^{KO} cells, it was abolished after the HA-MAD2 was turned off.

We next examined if the SAC could be rescued with a MAD2^{L13Q} mutant, which adopts the C-MAD2 conformation (Mapelli et al., 2007). FLAG-tagged MAD2^{L13Q} (or wild-type MAD2 control) was transfected into the MAD2^{KO} cells before the HA-MAD2 was silenced with Dox (Figure 6B). As anticipated, cells lacking MAD2 could not be arrested in mitosis with NOC (as indicated by histone H3^{Ser10} phosphorylation) (Figure 6C). Importantly, expression of wild-type FLAG-MAD2, but not MAD2^{L13Q}, was able to restore the histone H3^{Ser10} phosphorylation. Consistent with these results, wild-type, but not MAD2^{L13Q}, could form a complex with CDC20 during mitosis (Figure 6D).

Collectively, these results suggested that, instead of relying on C-MAD2 alone, a pool of O-MAD2 is essential for the SAC activation.

MAD2 Deficiency Induces More Severe Mitotic Defects Than that by the Lack of MAD2 Remodeling

The above results indicated that the SAC was non-functional in cells containing only C-MAD2 (TRIP13^{KO}) or in cells lacking

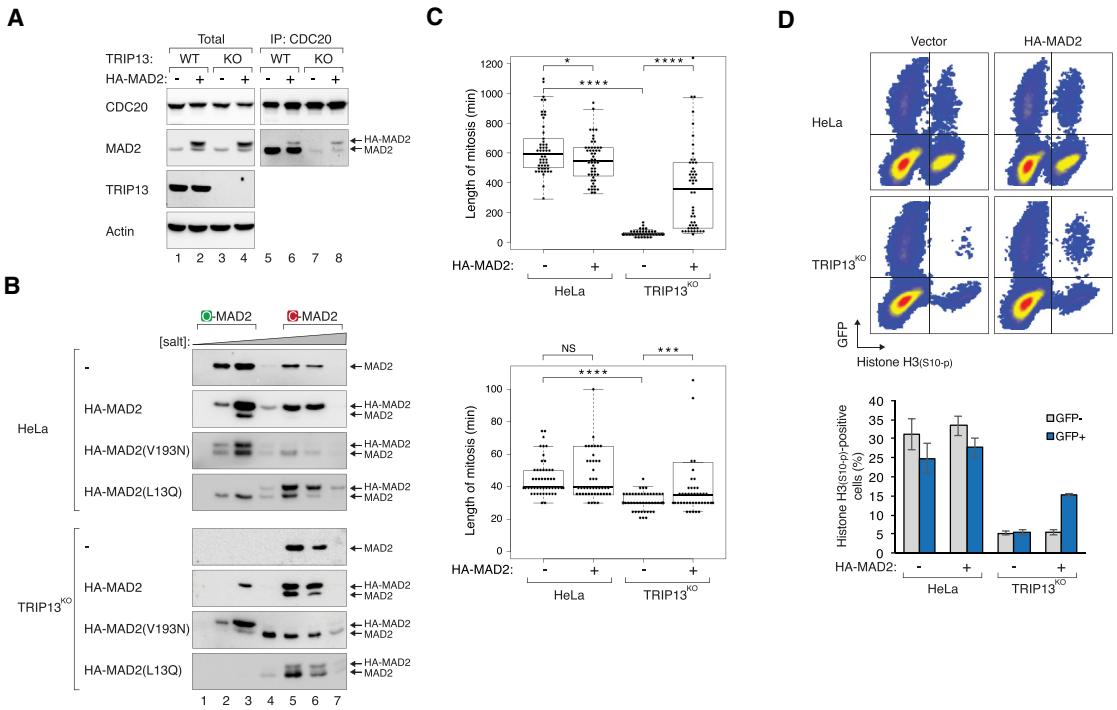

Figure 5. Ectopically Expressed MAD2 Restores O-MAD2 and Functional SAC in TRIP13-Deficient Cells

(A) Ectopically expressed MAD2 can bind CDC20 in the absence of TRIP13. HeLa (WT) and TRIP13^{KO} (KO) were synchronized with a double-thymidine protocol. After the first thymidine release, the cells were transfected with control plasmid or one expressing HA-MAD2. At 6 hr after the second thymidine release, the cells were incubated with a CDK1 inhibitor (RO3306) for 6 hr to trap them in G_2. The cells were then released from the RO3306 block and incubated with NOC and MG132 to arrest them in mitosis (harvested by mechanical shakeoff 2 hr later). Lysates were prepared and subjected to immunoprecipitation with antibodies against CDC20. Both the total lysates and the immunoprecipitates were analyzed with immunoblotting. The positions of HA-MAD2 and endogenous MAD2 are indicated.

(B) Ectopically expressed MAD2 is synthesized as O-MAD2 in the absence of TRIP13. HeLa and TRIP13^{KO} cells were synchronized and transfected with HA-MAD2 as in (A) and harvested when they were at G_2. Lysates were prepared and MAD2 conformation was analyzed using ion exchange chromatography as in Figure 1D. MAD2 mutants that only present in the C-MAD2 conformation (MAD2^{L13Q}) or the O-MAD2 conformation (Mapelli et al., 2007) were transfected as controls.

(C) Ectopically expressed MAD2 increases the length of mitosis in TRIP13^{KO} cells. HeLa and TRIP13^{KO} were transiently transfected with a control plasmid or one expressing HA-MAD2. A histone H2B-GFP-expressing plasmid was co-transfected to serve as a transfection marker. At 24 hr after transfection, the cells were incubated with NOC (upper panel) or buffer (lower panel) and analyzed with live-cell imaging for 24 hr. Box-and-whisker plots show the duration of mitosis (n = 50). *p < 0.05, ***p < 0.001, and ****p < 0.0001; NS, not significant. Examples of each treatment are shown in Movies S1, S2, S3, S4, S5, S6, S7, and S8).

(D) Ectopically expressed MAD2 increases the length of mitotic arrest in TRIP13^{KO} cells. HeLa and TRIP13^{KO} were transfected with HA-MAD2 as in (C). The cells were incubated with NOC for 6 hr, fixed, and stained with antibodies against histone H3^{Ser10} phosphorylation. The percentage histone H3^{Ser10} phosphorylation-positive cells in non-transfected (GFP-negative) and transfected (GFP-positive) cells was then analyzed using bivariate flow cytometry. Mean ± SEM of three independent experiments.

MAD2 altogether (MAD2^{KO}). Interestingly, TRIP13^{KO} cells (both HeLa and HCT116) displayed a relatively normal cell cycle (Ma and Poon, 2016), with the duration of unperturbed mitosis only marginally shorter than in TRIP13-containing cells (Figure 5C). By contrast, MAD2-deficient cells were not viable and could not be generated without rescuing them with recombinant MAD2. Figure 7A confirms that both MAD2- and TRIP13-deficient cells failed to activate the SAC when challenged with NOC. The knockout of MAD2 did not affect the expression of TRIP13. Likewise, the loss of the SAC in TRIP13^{KO} was not due to a reduction in MAD2. Figure 7B shows that apoptosis was induced after HA-MAD2 was turned off in MAD2^{KO} cells (as indicated by PARP1 cleavage), but not when AID-TRIP13 was turned off in TRIP13^{KO} cells. The increase in apoptosis in MAD2-deficient cells was further reflected in the deleterious effects on long-term cell viability (Figure 7C). These data indicated that, although the knockout of both MAD2 and TRIP13 abolished the SAC, only the deficiency in MAD2 promoted cell death during the unperturbed cell cycle.

To examine if the knockout of MAD2 and TRIP13 affected mitotic fidelity differently, anaphase cells were examined with microscopy. We found that missegregation of chromosomes, including lagging chromosomes and chromosome bridges, was dramatically increased in MAD2-deficient cells compared to control or TRIP13-deficient cells (Figure 7D). These data indicate a strong correlation between chromosome segregation defects and apoptosis in MAD2-deficient cells, which was absent in TRIP13-deficient cells. One possible explanation is that,

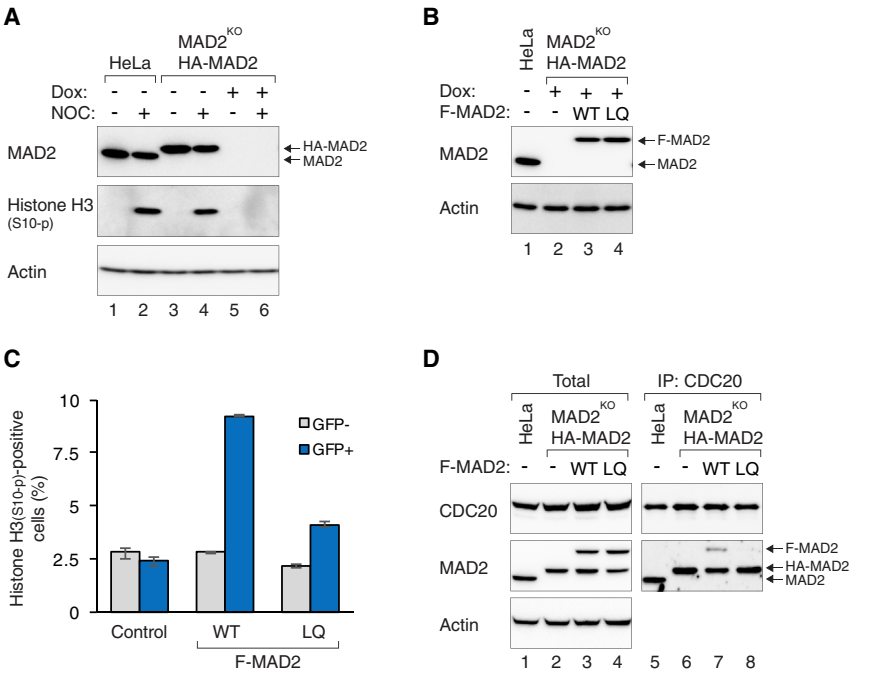

Figure 6. Recombinant C-MAD2 Alone Cannot Enable the SAC

(A) Knockout of MAD2 disrupts the SAC. MAD2^{KO} expressing HA-MAD2 was grown in the absence or presence of Dox for 24 hr to turn on or off the HA-MAD2, respectively. Both the HA-MAD2-expressing MAD2^{KO} and control HeLa cells were incubated with buffer or NOC. After 16 hr, lysates were prepared and analyzed with immunoblotting.

(B) Rescue of MAD2 deficiency with wild-type and mutant MAD2. MAD2^{KO} expressing HA-MAD2 was transfected with plasmids expressing FLAG-tagged MAD2. Either wild-type (WT) or a C-MAD2-specific mutant (LQ) was used. A histone H2B-GFP-expressing plasmid was co-transfected. The cells were then grown in the presence of Dox for 24 hr to turn off HA-MAD2, before being incubated with NOC for 6 hr. The expression of MAD2 was examined with immunoblotting. Lysates of HeLa cells were loaded to the indicated position of the endogenous MAD2.

(C) Wild-type, but not C-MAD2-specific, MAD2 restores the SAC in MAD2-deficient cells. MAD2^{KO} expressing HA-MAD2 was transfected with plasmids expressing FLAG-MAD2 (either WT or LQ) and treated with Dox and NOC as described in (B). The cells were fixed and the expression of histone H3^{Ser10} phosphorylation in transfected (GFP-positive) and untransfected (GFP-negative) cells was analyzed with flow cytometry. Mean ± SEM of three independent experiments.

(D) C-MAD2-specific mutant cannot form a complex with CDC20. MAD2^{KO} expressing HA-MAD2 was synchronized using a double-thymidine method. The cells were transiently transfected with plasmids expressing FLAG-tagged MAD2 (either WT or LQ) after the first thymidine release. At 9 hr after transfection, fresh medium and thymidine were applied to enforce the second thymidine block. At 8 hr after the second thymidine release, the cells were treated with NOC for 4 hr. Lysates were prepared and subjected to immunoprecipitation with antibodies against CDC20. Lysates of HeLa cells were also used as a control. Both the total lysates and immunoprecipitates were analyzed with immunoblotting.

although the C-MAD2 present in TRIP13-deficient cells could not support the SAC, newly synthesized MAD2 provided sufficient O-MAD2 to enable the SAC for unperturbed mitosis. In agreement with this, a small but detectable portion of MAD2 (~1%) was in O-MAD2 form in TRIP13^{KO} cells (Figures 1D and S3B). Collectively, these data indicated that the loss of MAD2 remodeling induces a different degree of aberrant mitosis and chromosomal instability compared to the loss of MAD2.

DISCUSSION

In this study, we demonstrated that, after AID-TRIP13 was targeted to degradation, NOC was still able to trap the TRIP13-deficient cells in mitosis (Figures 1 and 2). The formation of the MCC was also unaffected immediately after the destruction of TRIP13 (Figures 3B and S2). Importantly, this occurred before all the O-MAD2 was converted to C-MAD2 (Figures 1D and 3A). The SAC only became impaired about one to two cell cycles after TRIP13 was removed, correlating with the gradual depletion of O-MAD2 (Figures 1C and 1D). While some O-MAD2 was likely to convert to C-MAD2 as cells pass through mitosis (Figure 3A), O-MAD2 is also known to convert to C-MAD2 during interphase in MCC formation (Musacchio, 2015) as well as spontaneously with slow kinetics (Faesen et al., 2017; Luo et al., 2004). Collectively, our data indicate that the absence of the SAC in TRIP13-deficient cells may be due to an indirect effect of TRIP13 loss.

Several pieces of evidence indicate that gradual O-MAD2 depletion is the underlying mechanism of SAC impairment in TRIP13-deficient cells. First, ectopic overexpression of MAD2 appeared to generate sufficient O-MAD2 in the TRIP13^{KO} background (Figure 5B) to restore MAD2-CDC20 complexes (Figure 5A) and SAC-mediated mitotic arrest (Figures 5C and 5D). In agreement with this, prolonged mitotic block can be induced in TRIP13-ablated human RPE-2 cells overexpressing MAD2 (Marks et al., 2017). Second, the C-MAD2-specific MAD2^{L13Q} mutant was unable to rescue the CDC20 binding and SAC defects caused by MAD2 knockout (Figure 6). The inability of C-MAD2 alone to activate the SAC is also reflected in the reduction of MAD2 recruitment to unattached kinetochores (Nelson et al., 2015; Yost et al., 2017). The remaining MAD2 at unattached kinetochores was likely to represent MAD1–C-MAD2 complexes. Indeed, the abundance of MAD1-MAD2 complexes was not affected by TRIP13 (Figure 3B). These data are consistent with a model that, while MAD1 can bind C-MAD2 directly at the kinetochore, the second molecule of MAD2 that binds MAD1-MAD2 has to be O-MAD2. In the absence of O-MAD2 (for example in TRIP13^{KO}), there was a dramatic increase in p31^{comet} binding to MAD1-MAD2 (Figure 3C). Nevertheless, this probably does not contribute to the loss of the SAC in TRIP13^{KO} cells, as TRIP13^{KO} p31^{KO} double-knockout cells are also defective in the SAC (Ma and Poon, 2016).

Our data are consistent with the model that unliganded C-MAD2 alone is inadequate to function as an APC/C inhibitor.

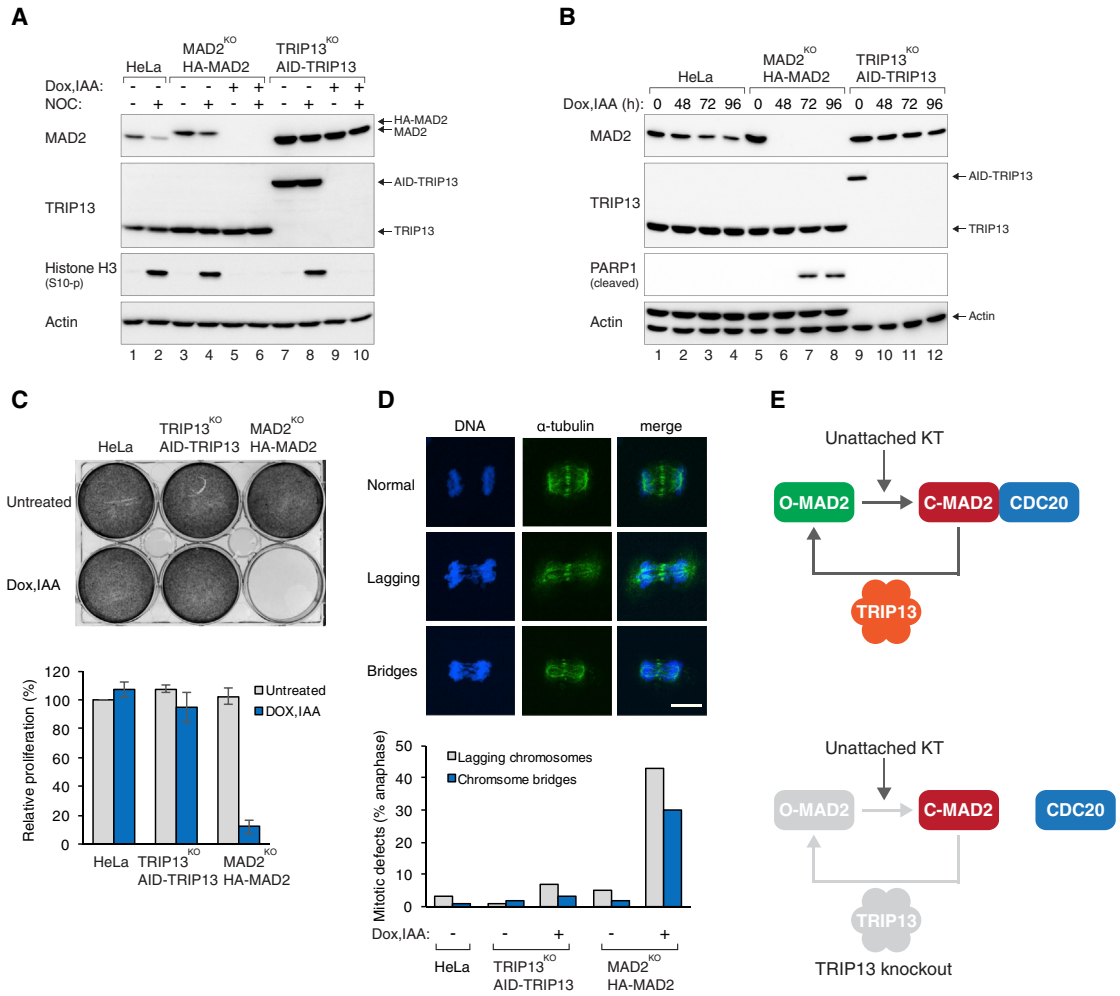

Figure 7. MAD2 Deficiency Induces More Severe Mitotic Aberrations Than that by the Lack of MAD2 Remodeling

(A) Deficiency in either MAD2 or TRIP13 induces a defective SAC. HeLa, MAD2^{KO} expressing HA-MAD2, and TRIP13^{KO} expressing AID-TRIP13 were incubated with buffer or IAA and Dox for 36 hr. The cells were then challenged with either buffer or NOC. After 16 hr, lysates were prepared and analyzed with immunoblotting.

(B) Deficiency in MAD2, but not TRIP13, promotes cell death. HeLa, MAD2^{KO} expressing HA-MAD2, and TRIP13^{KO} expressing AID-TRIP13 were incubated with buffer or IAA and Dox. The cells were harvested at the indicated time points. The expression of the indicated proteins was detected with immunoblotting. The upper bands in the actin blot were signals from the TRIP13 blot.

(C) Deficiency in MAD2, but not TRIP13, suppresses cell proliferation. HeLa, TRIP13^{KO} expressing AID-TRIP13, and MAD2^{KO} expressing HA-MAD2 were plated (20,000 cells per well on 6-well plates), and the cells were grown in the absence or presence of IAA and Dox for 6 days. The cells were then fixed and visualized by staining with crystal violet. The signals were quantified using ImageLab software (Bio-Rad, Hercules, CA, USA). Mean ± SEM of three independent experiments. A representative experiment is shown at the top. Relative proliferation was normalized to untreated HeLa cells.

(D) Severe chromosome segregation lesions in MAD2-deficient cells. HeLa, MAD2^{KO} expressing HA-MAD2, and TRIP13^{KO} expressing AID-TRIP13 were incubated with buffer or IAA and Dox. After 48 hr, the cells were fixed, stained with antibodies against α-tubulin and Hoechst 33258 (DNA), before being examined using a spinning-disk confocal microscope. The percentage of anaphase cells containing chromosome segregation defects was quantified (n = 50; mean of two independent experiments). Examples of normal anaphase and anaphase displaying lagging chromosomes or chromosome bridges are shown. Scale bar, 10 μm.

(E) A model of the role of TRIP13-mediated MAD2 conversion in the SAC. Unattached kinetochores (KTs) recruit O-MAD2 to MAD1–C-MAD2 complexes and facilitate the conversion of the O-MAD2 into C-MAD2. This process is likely to be directly coupled to CDC20 binding. TRIP13 replenishes the O-MAD2 pool so that it can be activated by unattached kinetochores. In the absence of TRIP13 (lower panel), the O-MAD2 pool is consequently depleted over time. In spite of the presence of C-MAD2, it is not incorporated into CDC20 complexes without O- to C-MAD2 conversion. Hence, the SAC cannot be activated in TRIP13-deficient cells.

Instead, the conversion of O- to C-MAD2 is directly coupled to CDC20 binding. Previous studies of TRIP13 mainly focus on its potential role in O- to C-MAD2 conversion for mitotic exit (Eytan et al., 2014; Ye et al., 2015, 2017; Wang et al., 2014). An implication of our model is that a major function of TRIP13 is to replenish the O-MAD2 pool so that it can be activated by unattached kinetochores (Figure 7E).

When HA-MAD2 was ectopically expressed in TRIP13^{KO} cells, it could bind CDC20 and partially restore NOC-induced mitotic block (Figure 5). We believe that, because the newly synthesized

HA-MAD2 contained O-MAD2 (Figure 5B), it could facilitate the SAC in these cells. In support of this, the HA-MAD2, but not the endogenous MAD2, was incorporated into CDC20 complexes (Figure 5A). The relative inefficiency of the rescue of the SAC was probably due to the continued conversion of O-MAD2 into C-MAD2 both during mitosis and interphase.

Unliganded C-MAD2 is hypothesized to function in the SAC in the two-state MAD2 model (Luo et al., 2004) and the conformational activation model (Luo and Yu, 2008). Both models emphasize the roles of unliganded C-MAD2 releasing from the kinetochore for CDC20 binding, which is supported by several pieces of *in vitro* data. For example, purified recombinant MAD1-MAD2 complexes can stimulate the conversion of O-MAD2 to unliganded C-MAD2 in the absence of CDC20 (Yang et al., 2008). Moreover, overexpressed $MAD2^{L13A}$ (a C-MAD2-specific mutant) is more efficient in promoting mitotic arrest than wild-type MAD2 (Yang et al., 2008). Nevertheless, whether unliganded C-MAD2 exists in normal human cells remains elusive (Luo and Yu, 2008). Our data indicated that, although C-MAD2 was present in $TRIP13^{KO}$ cells and did not bind CDC20, some of the C-MAD2 molecules were associated with MAD1 (Figure 3C) and $p31^{comet}$ (Figure 3B). As we previously showed that removal of MAD1 from $TRIP13^{KO}$ lysates by immunodepletion only slightly reduces the total MAD2 (Ma and Poon, 2016), it is likely that unliganded C-MAD2 was present in $TRIP13^{KO}$ cells but remained non-functional.

Our data are in general consistent with the MAD2 template model, in which MAD1–C-MAD2 at the kinetochores serves as a template to bind O-MAD2 and convert it into C-MAD2 (De Antoni et al., 2005). The C-MAD2 then binds CDC20, which in turn may serve as a template for converting more O-MAD2 into C-MAD2 in the cytosol (Luo et al., 2002). Several pieces of *in vitro* evidence support the idea that the remodeling of O- to C-MAD2 occurs concomitantly with the binding to CDC20 (Kulukian et al., 2009; Simonetta et al., 2009; Faesen et al., 2017). For example, MAD1–C-MAD2 significantly accelerates the binding of O-MAD2 to CDC20 *in vitro* (Kulukian et al., 2009; Simonetta et al., 2009). Nevertheless, direct evidence supporting this hypothesis in cells has yet to be established. Given that CDC20 is enriched at kinetochores during mitosis (Howell et al., 2004; Kallio et al., 1998, 2002), the proximity to MAD1-MAD2 may provide a mechanism to couple MAD2 to CDC20 after C-MAD2 is generated.

Given the essential role of TRIP13 in converting C-MAD2 to O-MAD2, it is anticipated that it plays a key role in inactivating the SAC to facilitate mitotic exit. But as the SAC cannot be activated in the absence of TRIP13, it was previously not possible to formally show that TRIP13 is involved in SAC inactivation during mitotic exit. The auxin-dependent degron system described here allowed us to inactivate TRIP13 only after mitotic block and investigate the role of TRIP13 specifically in mitotic exit. Interestingly, we found that the degradation of TRIP13 during mitosis merely deferred mitotic exit from ~40 to ~80 min (unpublished data). This suggested that, at least for the cancer cells we used as models, TRIP13 is not the sole mechanism for SAC inactivation. A number of alternative mechanisms have been proposed, including the ubiquitination and degradation of CDC20, removal of checkpoint components from kinetochores by a dynein-mediated mechanism, and action of phosphatases (Musacchio, 2015). Recently, a CCT chaperonin has also been shown to be able to disassemble the MCC (Kaisari et al., 2017).

A perplexing finding is that, although both $TRIP13^{KO}$ and $MAD2^{KO}$ lacked a functional SAC, they displayed a very different degree of chromosomal instability during unperturbed mitosis (Figure 7D). This was reflected in the detrimental effects on cell proliferation in $MAD2^{KO}$ cells (Figures 7B and 7C). Consistent with these results, while *Mad2*-knockout mice are embryonic lethal (Dobles et al., 2000), *Trip13*-knockout mice (generated with gene trap techniques and contained vastly reduced level of Trip13) are born at ~2/3 the expected ratio but are otherwise grossly normal (Li and Schimenti, 2007). Aneuploidy during early development (which is a major cause of human spontaneous abortion) may underlie the decreased birth rate in *Trip13*-knockout mice. We speculate that, although $TRIP13^{KO}$ cells are incapable of regenerating O-MAD2, there is a sufficient amount of O-MAD2 in newly synthesized MAD2 (Figures 1D and S3B) to facilitate unperturbed mitosis. Notably, these results imply that mutations of various components of the SAC may have distinct effects on mitosis. A caveat is that, as the cancer cells used in this study already exhibited extensive aneuploidy, it is possible that a limited increase in aneuploidy can be tolerated by cancer cells (Foijer et al., 2017). Another possibility is that the effects of SAC impairment could be cell type specific. For example, Mad2 deficiency is tolerated by mouse epidermal cells, but not hair follicle stem cells (Foijer et al., 2013).

A dysregulated SAC promotes aneuploidy, a hallmark of many cancers and birth defects. Given that the loss of TRIP13 disrupts the SAC via depletion of O-MAD2, an immediate implication of this study is on the mechanism of chromosomal instability in cancers containing TRIP13 mutations. Indeed, individuals with loss-of-function mutations in TRIP13 show impaired SAC and are predisposed to Wilms tumor (Yost et al., 2017). It is likely that depletion of O-MAD2 is one of the mechanisms of SAC failure in these cancers. A prediction is that ectopic expression of MAD2 in these cells may increase O-MAD2 and restore the SAC (Figure 5). In this connection, cancer cells overexpressing MAD2 are sensitive to TRIP13 reduction in cell proliferation and tumor xenograft assays (Marks et al., 2017). As regulation of MAD2 is only one of the many functions attributed to TRIP13 (Vader, 2015), it is conceivable that TRIP13 deficiency can contribute to tumorigenesis via processes other than mitosis. Moreover, MAD2 (as well as $p31^{comet}$ and BUBR1) has been shown to function in insulin signaling (Choi et al., 2016). Hence, it is also possible that TRIP13-mediated MAD2 remodeling can affect non-mitotic processes, such as metabolism.

EXPERIMENTAL PROCEDURES

DNA Constructs

TRIP13 CRISPR-Cas9 construct was generated as described previously (Ma and Poon, 2016). As the PAM sequence of TRIP13 CRISPR-Cas9 spanned the UTR, the AID-TRIP13 construct was not targeted. To generate an AID construct in Tet-Off system (pUHD-AID), an internal NcoI site in the AID cDNA was mutated by the double-PCR procedure using 5′-AAGCT AGCATGGGCAGTGTCGAG-3′, 5′-GTTTGCCCATCGTAAAAGAGCTG-3′ and

5′-TCAGCTCTTTTACGATGGGCAAAC-3′, and 5′-CACCATGGTGAATAGGA TATCGGCA-3′ using pMK106 (Nishimura et al., 2009) as the template. The PCR product was digested with NheI and NcoI and ligated to the NheI-NcoI-cut pUHD-P3/PUR (Ma et al., 2009). To generate AID-TRIP13 retrovirus constructs, the XhoI-NcoI fragment from pUHD-AID and the NcoI-BamHI from FLAG-TRIP13 in pUHD-P3 (Ma and Poon, 2016) were ligated into a modified pRevTRE2 (lacking an XhoI site) (Clontech Laboratories, Palo Alto, CA, USA). MAD2 CRISPR-Cas9 targeting GATTTCGGCGCTCCCGCGCA was prepared by ligating the annealing product of 5′-CACCGATTTCGGCGCTCC CGCGCA-3′and 5′-AAACTGCGCGGGAGCGCCGAAATC-3′ to pX330 (obtained from Addgene) cut with BbsI. HA-MAD2 in pUHD-P2 was constructed as previously described (Ma et al., 2007). A puromycin-resistant cassette was inserted into the HindIII site to create HA-MAD2 in pUHD-P2/PUR. To generate the CRISPR-resistant MAD2 expression construct, the silent mutations in the CRISPR-Cas9-targeting region (GATTTCGGCGGATCCGCGCA) and PAM sequence (CAC) were introduced in the cDNA: the PCR products of 5′-AGCTCGTTTAGTGAACCGTCAGATCG-3′, 5′-AAGGATCCGCGCAGTGT GATTCCC-3′ and 5′-AAGGATCCGCCGAAATCGTGG-3′, and 5′-TATCTTAT CATGTCTGGATCC-3′ using HA-MAD2 in pUHD-P2/PUR as a template were digested with EcoRI, BamHI and BamHI, and XbaI, respectively, and then ligated to EcoRI-XbaI-digested pUHD-P2/PUR. To prepare the FLAG-MAD2-myc-H6 construct, MAD2-myc-H6 was first prepared by ligating the BamHI-EcoRI-cut PCR product (5′-GGGATCCATGGCGCTGCAGCTCT-3′ and 5′-TGAATTCCCCAGTCATTGACAGGA-3′ using HA-MAD2 in pUHD-P2 as template) into BamHI-EcoRI-cut pcDNA3.1/myc-HisC (Life Technologies, Carlsbad, CA, USA). The NcoI-BamHI-cut PCR product (5′-GGGATC CATGGCGCTGCAGCTCT-3′ and 5′-GAGGATCCTAGAAGGCACAGTCGA GGC-3′ using MAD2-myc-H6 in pcDNA3.1/myc-HisC as template) was ligated into NcoI-BamHI-cut pUHD-P3/PUR to create FLAG-MAD2-myc-H6 in pUHD-P3/PUR. The L13Q mutation was introduced as previously described (Ma and Poon, 2016). HA-MAD2^{V193N} was generated similarly as HA-MAD2^{L13Q} using the oligonucleotides 5′-CACAAAAACAATAGCATGGTGGCCTACAA-3′ and 5′-GCTATTGTTTTTGTGGATTGTAGTAGTAA-3′. To generate the TIR1-myc retrovirus constructs, the BglII-XhoI-cut product of pMK106 was ligated to BamHI-SalI-digested pBabe-puro (a gift from Jade Shi, Hong Kong Baptist University). Histone H2B-GFP retroviral construct was a gift from George Tsao (The University of Hong Kong).

Cell Culture

The HeLa used in this study was a clone that expressed the tTA tetracycline transactivator (Yam et al., 2000). TRIP13^{KO} cells were generated as previously described (Ma and Poon, 2016). AID-TRIP13 in TRIP13^{KO} or in TRIP13^{KO} p31^{KO} was generated by infecting cells (HeLa or p31^{KO}, respectively; Ma and Poon, 2016) with retroviruses expressing AID-TRIP13, followed by TRIP13 CRIPSR-Cas9-mediated knockout and TIR1 infection. Some clones of AID-TRIP13 in TRIP13^{KO} were also generated by first transfecting TRIP13 CRISPR-Cas9 before infecting with the AID-TRIP13 and TIR1-myc constructs. To generate MAD2^{KO} cells, HeLa cells were transfected with MAD2 CRISPR-Cas9 in pX330 and HA-MAD2 in pUHD-P2/PUR plasmids. The transfected cells were selected by growing in puromycin-containing medium for 10 days followed by drug-free medium for 5 days. The MAD2 CRISPR-Cas9 was transfected a second time together with a plasmid expressing blasticidin-resistant gene (gift from Tim Hunt). The transfected cells were selected by growing in blasticidin-containing medium for 2 days. The cells were then seeded onto 96-well plates with limiting dilution to obtain single cell-derived colonies. The colonies were then analyzed with immunoblotting to confirm successful gene disruption and expression of HA-MAD2.

Cells were transfected with plasmids using a calcium phosphate precipitation method (Ausubel et al., 1995). Cells were treated with the following reagents at the indicated final concentration: Dox (2 μg/mL), IAA (50 μg/mL) (Sigma-Aldrich, St. Louis, MO, USA), MG132 (10 μM), AZ3146 (2 μM) (Selleck Chemicals, Houston, TX, USA), nocodazole (0.33 μM), and RO3306 (10 μM) (Enzo Life Sciences, Farmingdale, NY, USA).

Cell Cycle Synchronization

Cell cycle synchronization using a double-thymidine method was performed as described (Ma and Poon, 2011a).

Live-Cell Imaging and Microscopy

The setup and conditions of time-lapse microscopy of living cells were as described previously (Mak et al., 2015). To analyze lagging chromosomes and chromosome bridges, cells growing on coverslips were fixed with 2% paraformaldehyde for 10 min at 25°C. The samples were blocked and permeabilized with 2% BSA and 0.5% Triton X-100 in PBS for 30 min, incubated with antibodies against α-tubulin (Abcam, Cambridge, UK) at 25°C for 2 hr, before being incubated with secondary antibodies (Alexa Fluor565 goat anti-Rabbit IgG antibody, Life Technologies) at 25°C for 2 hr. DNA was stained with Hoechst 33258. The samples were then washed three time with PBS containing 0.1% Triton X-100 prior to mounting. Images were acquired using a Revolution XDi laser-based spinning-disk microscopy system (Andor, Belfast, UK).

Flow Cytometry Analysis

Analysis of DNA contents and histone H3^{Ser10} phosphorylation using flow cytometry was performed as previously described (Ma and Poon, 2011a).

Antibodies and Immunological Methods

Antibodies against β-actin (Sigma-Aldrich), APC4 (Abcam), BUBR1 (Bethyl Laboratories, Montgomery, TX, USA), CDC20, MAD1, phospho-histone H3^{Ser10}, TRIP13 (Santa Cruz Biotechnology, Santa Cruz, CA, USA), cleaved PARP1(Asp214), MAD2 (BD Transduction Laboratories, Franklin Lakes, NJ, USA), and MPM2 (Calbiochem, San Diego, CA, USA) were obtained from the indicated suppliers. Antibodies against cyclin B1 were gifts from Julian Gannon (Cancer Research UK). Polyclonal antibodies against MAD2 (Ma and Poon, 2011b) and p31^{comet} (Ma et al., 2012) were prepared as previously described. Immunoblotting was performed as previously described (Ma and Poon, 2016). Band intensity was quantified using Image Lab software (Bio-Rad, Hercules, CA, USA). Immunoprecipitation was performed as described (Ma et al., 2012).

MAD2 Conformation Analysis

MAD2 conformation was determined using spin column-based ion exchange chromatography as previously described (Ma and Poon, 2016).

Statistical Analysis

Box-and-whisker plots (center lines show the medians; box limits indicate interquartile range; whiskers extend 1.5 times the interquartile range from the 25th and 75th percentiles) were generated by RStudio (Boston, MA, USA). Mann-Whitney-Wilcoxon test was used to calculate statistical significance (*$p < 0.05$, ***$p < 0.001$, and ****$p < 0.0001$).

SUPPLEMENTAL INFORMATION

Supplemental Information includes six figures and eight movies and can be found with this article online at https://doi.org/10.1016/j.celrep.2018.01.027.

ACKNOWLEDGMENTS

This work was supported in part by the RGC grant 16100017 and HMRF grant 04153526 (to H.T.M.) and RGC grant T12-704/16-R and Innovation and Technology Commission grant ITCPD/17-9 (to R.Y.C.P.).

AUTHOR CONTRIBUTIONS

H.T.M. and R.Y.C.P. conceived the project and designed experiments. H.T.M. carried out experiments. H.T.M. and R.Y.C.P. analyzed the data and wrote the manuscript.

DECLARATION OF INTERESTS

The authors declare no competing interests.

Received: August 12, 2017
Revised: December 10, 2017
Accepted: January 10, 2018
Published: February 6, 2018

REFERENCES

Alfieri, C., Chang, L., Zhang, Z., Yang, J., Maslen, S., Skehel, M., and Barford, D. (2016). Molecular basis of APC/C regulation by the spindle assembly checkpoint. Nature *536*, 431–436.

Ausubel, F.M., Brent, R., Kingston, R.E., Moore, D.D., Seidman, J.G., Smith, J.A., and Struhl, K. (1995). Current Protocols in Molecular Biology (Massachusetts General Hospital, Harvard Medical School).

Choi, E., Zhang, X., Xing, C., and Yu, H. (2016). Mitotic Checkpoint Regulators Control Insulin Signaling and Metabolic Homeostasis. Cell *166*, 567–581.

De Antoni, A., Pearson, C.G., Cimini, D., Canman, J.C., Sala, V., Nezi, L., Mapelli, M., Sironi, L., Faretta, M., Salmon, E.D., and Musacchio, A. (2005). The Mad1/Mad2 complex as a template for Mad2 activation in the spindle assembly checkpoint. Curr. Biol. *15*, 214–225.

Dobles, M., Liberal, V., Scott, M.L., Benezra, R., and Sorger, P.K. (2000). Chromosome missegregation and apoptosis in mice lacking the mitotic checkpoint protein Mad2. Cell *101*, 635–645.

Eytan, E., Wang, K., Miniowitz-Shemtov, S., Sitry-Shevah, D., Kaisari, S., Yen, T.J., Liu, S.T., and Hershko, A. (2014). Disassembly of mitotic checkpoint complexes by the joint action of the AAA-ATPase TRIP13 and p31(comet). Proc. Natl. Acad. Sci. USA *111*, 12019–12024.

Faesen, A.C., Thanasoula, M., Maffini, S., Breit, C., Müller, F., van Gerwen, S., Bange, T., and Musacchio, A. (2017). Basis of catalytic assembly of the mitotic checkpoint complex. Nature *542*, 498–502.

Foijer, F., DiTommaso, T., Donati, G., Hautaviita, K., Xie, S.Z., Heath, E., Smyth, I., Watt, F.M., Sorger, P.K., and Bradley, A. (2013). Spindle checkpoint deficiency is tolerated by murine epidermal cells but not hair follicle stem cells. Proc. Natl. Acad. Sci. USA *110*, 2928–2933.

Foijer, F., Albacker, L.A., Bakker, B., Spierings, D.C., Yue, Y., Xie, S.Z., Davis, S., Lutum-Jehle, A., Takemoto, D., Hare, B., et al. (2017). Deletion of the MAD2L1 spindle assembly checkpoint gene is tolerated in mouse models of acute T-cell lymphoma and hepatocellular carcinoma. eLife *6*, e20873.

Habu, T., Kim, S.H., Weinstein, J., and Matsumoto, T. (2002). Identification of a MAD2-binding protein, CMT2, and its role in mitosis. EMBO J. *21*, 6419–6428.

Howell, B.J., Moree, B., Farrar, E.M., Stewart, S., Fang, G., and Salmon, E.D. (2004). Spindle checkpoint protein dynamics at kinetochores in living cells. Curr. Biol. *14*, 953–964.

Izawa, D., and Pines, J. (2015). The mitotic checkpoint complex binds a second CDC20 to inhibit active APC/C. Nature *517*, 631–634.

Ji, Z., Gao, H., Jia, L., Li, B., and Yu, H. (2017). A sequential multi-target Mps1 phosphorylation cascade promotes spindle checkpoint signaling. eLife *6*, e22513.

Kaisari, S., Sitry-Shevah, D., Miniowitz-Shemtov, S., Teichner, A., and Hershko, A. (2017). Role of CCT chaperonin in the disassembly of mitotic checkpoint complexes. Proc. Natl. Acad. Sci. USA *114*, 956–961.

Kallio, M., Weinstein, J., Daum, J.R., Burke, D.J., and Gorbsky, G.J. (1998). Mammalian p55CDC mediates association of the spindle checkpoint protein Mad2 with the cyclosome/anaphase-promoting complex, and is involved in regulating anaphase onset and late mitotic events. J. Cell Biol. *141*, 1393–1406.

Kallio, M.J., Beardmore, V.A., Weinstein, J., and Gorbsky, G.J. (2002). Rapid microtubule-independent dynamics of Cdc20 at kinetochores and centrosomes in mammalian cells. J. Cell Biol. *158*, 841–847.

Kulukian, A., Han, J.S., and Cleveland, D.W. (2009). Unattached kinetochores catalyze production of an anaphase inhibitor that requires a Mad2 template to prime Cdc20 for BubR1 binding. Dev. Cell *16*, 105–117.

Li, X.C., and Schimenti, J.C. (2007). Mouse pachytene checkpoint 2 (trip13) is required for completing meiotic recombination but not synapsis. PLoS Genet. *3*, e130.

Luo, X., and Yu, H. (2008). Protein metamorphosis: the two-state behavior of Mad2. Structure *16*, 1616–1625.

Luo, X., Tang, Z., Rizo, J., and Yu, H. (2002). The Mad2 spindle checkpoint protein undergoes similar major conformational changes upon binding to either Mad1 or Cdc20. Mol. Cell *9*, 59–71.

Luo, X., Tang, Z., Xia, G., Wassmann, K., Matsumoto, T., Rizo, J., and Yu, H. (2004). The Mad2 spindle checkpoint protein has two distinct natively folded states. Nat. Struct. Mol. Biol. *11*, 338–345.

Ma, H.T., and Poon, R.Y. (2011a). Synchronization of HeLa cells. Methods Mol. Biol. *761*, 151–161.

Ma, H.T., and Poon, R.Y. (2011b). Orderly inactivation of the key checkpoint protein mitotic arrest deficient 2 (MAD2) during mitotic progression. J. Biol. Chem. *286*, 13052–13059.

Ma, H.T., and Poon, R.Y.C. (2016). TRIP13 Regulates Both the Activation and Inactivation of the Spindle-Assembly Checkpoint. Cell Rep. *14*, 1086–1099.

Ma, H.T., On, K.F., Tsang, Y.H., and Poon, R.Y. (2007). An inducible system for expression and validation of the specificity of short hairpin RNA in mammalian cells. Nucleic Acids Res. *35*, e22.

Ma, H.T., Tsang, Y.H., Marxer, M., and Poon, R.Y. (2009). Cyclin A2-cyclin-dependent kinase 2 cooperates with the PLK1-SCFbeta-TrCP1-EMI1-anaphase-promoting complex/cyclosome axis to promote genome reduplication in the absence of mitosis. Mol. Cell. Biol. *29*, 6500–6514.

Ma, H.T., Chan, Y.Y., Chen, X., On, K.F., and Poon, R.Y. (2012). Depletion of p31comet protein promotes sensitivity to antimitotic drugs. J. Biol. Chem. *287*, 21561–21569.

Mak, J.P., Man, W.Y., Chow, J.P., Ma, H.T., and Poon, R.Y. (2015). Pharmacological inactivation of CHK1 and WEE1 induces mitotic catastrophe in nasopharyngeal carcinoma cells. Oncotarget *6*, 21074–21084.

Mapelli, M., Filipp, F.V., Rancati, G., Massimiliano, L., Nezi, L., Stier, G., Hagan, R.S., Confalonieri, S., Piatti, S., Sattler, M., and Musacchio, A. (2006). Determinants of conformational dimerization of Mad2 and its inhibition by p31comet. EMBO J. *25*, 1273–1284.

Mapelli, M., Massimiliano, L., Santaguida, S., and Musacchio, A. (2007). The Mad2 conformational dimer: structure and implications for the spindle assembly checkpoint. Cell *131*, 730–743.

Marks, D.H., Thomas, R., Chin, Y., Shah, R., Khoo, C., and Benezra, R. (2017). Mad2 Overexpression Uncovers a Critical Role for TRIP13 in Mitotic Exit. Cell Rep. *19*, 1832–1845.

Musacchio, A. (2015). The Molecular Biology of Spindle Assembly Checkpoint Signaling Dynamics. Curr. Biol. *25*, R1002–R1018.

Nelson, C.R., Hwang, T., Chen, P.H., and Bhalla, N. (2015). TRIP13PCH-2 promotes Mad2 localization to unattached kinetochores in the spindle checkpoint response. J. Cell Biol. *211*, 503–516.

Nishimura, K., Fukagawa, T., Takisawa, H., Kakimoto, T., and Kanemaki, M. (2009). An auxin-based degron system for the rapid depletion of proteins in nonplant cells. Nat. Methods *6*, 917–922.

Primorac, I., and Musacchio, A. (2013). Panta rhei: the APC/C at steady state. J. Cell Biol. *201*, 177–189.

Simonetta, M., Manzoni, R., Mosca, R., Mapelli, M., Massimiliano, L., Vink, M., Novak, B., Musacchio, A., and Ciliberto, A. (2009). The influence of catalysis on mad2 activation dynamics. PLoS Biol. *7*, e10.

Skinner, J.J., Wood, S., Shorter, J., Englander, S.W., and Black, B.E. (2008). The Mad2 partial unfolding model: regulating mitosis through Mad2 conformational switching. J. Cell Biol. *183*, 761–768.

Vader, G. (2015). Pch2(TRIP13): controlling cell division through regulation of HORMA domains. Chromosoma *124*, 333–339.

Wang, K., Sturt-Gillespie, B., Hittle, J.C., Macdonald, D., Chan, G.K., Yen, T.J., and Liu, S.T. (2014). Thyroid hormone receptor interacting protein 13 (TRIP13) AAA-ATPase is a novel mitotic checkpoint-silencing protein. J. Biol. Chem. *289*, 23928–23937.

Yam, C.H., Siu, W.Y., Lau, A., and Poon, R.Y. (2000). Degradation of cyclin A does not require its phosphorylation by CDC2 and cyclin-dependent kinase 2. J. Biol. Chem. *275*, 3158–3167.

Yamaguchi, M., VanderLinden, R., Weissmann, F., Qiao, R., Dube, P., Brown, N.G., Haselbach, D., Zhang, W., Sidhu, S.S., Peters, J.M., et al. (2016). Cryo-EM of Mitotic Checkpoint Complex-Bound APC/C Reveals Reciprocal and Conformational Regulation of Ubiquitin Ligation. Mol. Cell *63*, 593–607.

Yang, M., Li, B., Tomchick, D.R., Machius, M., Rizo, J., Yu, H., and Luo, X. (2007). p31comet blocks Mad2 activation through structural mimicry. Cell *131*, 744–755.

Yang, M., Li, B., Liu, C.J., Tomchick, D.R., Machius, M., Rizo, J., Yu, H., and Luo, X. (2008). Insights into mad2 regulation in the spindle checkpoint revealed by the crystal structure of the symmetric mad2 dimer. PLoS Biol. *6*, e50.

Ye, Q., Rosenberg, S.C., Moeller, A., Speir, J.A., Su, T.Y., and Corbett, K.D. (2015). TRIP13 is a protein-remodeling AAA+ ATPase that catalyzes MAD2 conformation switching. eLife *4*, e07367.

Ye, Q., Kim, D.H., Dereli, I., Rosenberg, S.C., Hagemann, G., Herzog, F., Tóth, A., Cleveland, D.W., and Corbett, K.D. (2017). The AAA+ ATPase TRIP13 remodels HORMA domains through N-terminal engagement and unfolding. EMBO J. *36*, 2419–2434.

Yost, S., de Wolf, B., Hanks, S., Zachariou, A., Marcozzi, C., Clarke, M., de Voer, R., Etemad, B., Uijttewaal, E., Ramsay, E., et al. (2017). Biallelic TRIP13 mutations predispose to Wilms tumor and chromosome missegregation. Nat. Genet. *49*, 1148–1151.